

A new electromagnetic calorimeter for BabyIAXO to search for axions from solar fusion and supernova explosions

DESY Summer Student Report, September 22, 2025

Sarith Chopara, Mahidol University, Thailand

Abstract

This report summarises acceptance and shower-profile studies for a proposed electromagnetic calorimeter for BabyIAXO aimed at detecting MeV–100 MeV photons from solar fusion and supernova axion-related channels. Studies include: detector acceptance vs geometry, material and position (vacuum vs air) for 5.5 MeV and 100 MeV photons, application of Gaussian energy-resolution smearing, and shower-shape comparisons between gamma events and cosmic-muon backgrounds. The results inform detector material choice and placement (inside/outside cryostat).

Contents

1 Introduction **2**
- 1.1 Axion motivation and experimental context . . . 2
- 1.2 Solar and astrophysical production channels relevant to calorimetry . . . 2
- 1.3 Helioscope detection principle and calorimetry role . . . 3
- 1.4 BabyIAXO and experimental status . . . 3

2 Objectives **3**

3 Acceptance Study **5**
- 3.1 Methodology . . . 5
- 3.2 Energy resolution (Gaussian sampling) . . . 6
- 3.3 Acceptance calculation . . . 6
- 3.4 Results . . . 7

4 Shower Profile Study **7**
- 4.1 Methodology . . . 7
- 4.2 Results . . . 10
- 4.3 Key observations . . . 10

5 Conclusions **11**

1 Introduction

1.1 Axion motivation and experimental context

Axions are hypothetical pseudo–Nambu–Goldstone bosons introduced to solve the strong CP problem in quantum chromodynamics (QCD) through the Peccei–Quinn mechanism ([1]). When the global $U(1)_{\mathrm{PQ}}$ symmetry is spontaneously broken, an associated pseudo-scalar field — the axion — appears and dynamically relaxes the effective QCD CP-violating parameter $\bar{\theta}$ to zero, thereby explaining the non-observation of a neutron electric dipole moment. Seminal theoretical developments are given in [1], [2] and [3].

Beyond the original "QCD axion", the broader category of axion-like particles (ALPs) appears in many extensions of the Standard Model (string compactifications, extended Higgs sectors, etc.) ([4], [5]). Both QCD axions and ALPs generically couple to two photons via the effective Lagrangian term

$$\mathcal{L}_{a\gamma} = -\frac{1}{4} g_{a\gamma} a F_{\mu\nu} \tilde{F}^{\mu\nu} = g_{a\gamma} a \, \mathbf{E} \cdot \mathbf{B}, \tag{1}$$

where $g_{a\gamma}$ parametrises the axion—photon coupling strength. Axions may also couple to fermions (axion–nucleon coupling g_{aN}, axion–electron coupling g_{ae}) ([6], [7], [8], and [9]) with model-dependent strengths, opening multiple production and detection channels.

Axions and ALPs are motivated both as solutions to a theoretical puzzle (strong CP) and as viable dark-matter or particle candidates that can be produced in astrophysical environments. Observations and constraints from stellar cooling, supernova 1987A, and laboratory searches have shaped the viable parameter space; reviews and phenomenological summaries can be found in [10] and [11].

In a transverse magnetic field $\mathbf{B}_T$, axion–photon mixing leads to a conversion probability (for relativistic axions) approximated by

$$P_{a\to\gamma} \simeq \left(\frac{g_{a\gamma} B_T}{2}\right)^2 L^2 \frac{\sin^2(qL/2)}{(qL/2)^2}, \tag{2}$$

where q is the momentum transfer difference between axion and photon in the medium.

1.2 Solar and astrophysical production channels relevant to calorimetry

Photons arriving at a calorimeter in the vicinity of a helioscope can originate from multiple processes related to axions:

1. **Nuclear de-excitation / nuclear reaction lines:** axions (or ALPs) can be emitted in nuclear transitions and certain fusion reactions. For example, a well-known photon line in the Sun occurs from the radiative capture reaction $p + d \to {}^3\mathrm{He} + \gamma$ which produces a $\sim 5.5\,\mathrm{MeV}$ gamma; an axion analogue could be emitted if axion–nucleon couplings are present. Other nuclear lines (e.g. transitions in ${}^{57}\mathrm{Fe}$ producing 14.4 keV photons) have been considered in dedicated searches. These narrow-line channels provide opportunities for calorimetric detection at discrete energies [12].

2. **Supernova and transient sources:** core-collapse supernovae produce a large flux of axions via nucleon–nucleon bremsstrahlung and other processes; axion conversion or decay could generate high-energy photons (tens to hundreds of MeV) observable by a calorimeter. Constraints from SN1987A already set important limits on axion–nucleon couplings, but detection of axion-related gamma rays from a nearby future supernova remains a compelling possibility [13].

1.3 Helioscope detection principle and calorimetry role

Helioscopes (e.g. CAST [14], proposed IAXO [15]/BabyIAXO [16]) exploit the inverse-Primakoff effect: axions traversing a transverse magnetic field convert into X-ray photons with a probability depending on $g_{a\gamma}$, the magnetic-field strength B, the length L of the conversion region, and the optical properties of the propagation medium. The classic helioscope concept focuses on keV-range X-rays because of the inverse-Primakoff effect, detected with low-background X-ray detectors. A dedicated electromagnetic calorimeter expands the search reach to higher photon energies (MeV–100 MeV) from nuclear-line axions or transient astrophysical axion signals.
Calorimetry in this context has several complementary objectives:

- **High-energy line sensitivity:** resolve narrow gamma lines (e.g. $\sim$5.5 MeV) that could arise from axion-related nuclear processes. Excellent energy resolution and low threshold are required to separate signal from continuum background.
- **Angular acceptance and geometric considerations:** calorimeter placement (inside the cryostat vacuum vs outside behind structural materials) strongly affects acceptance at low energies where attenuation and conversion in front materials matter.
- **Background rejection through topology:** at MeV energies, electromagnetic showers and cosmic-ray muons exhibit different spatial and longitudinal energy-deposition patterns; a segmented calorimeter can exploit these differences to reduce background.

1.4 BabyIAXO and experimental status

BabyIAXO is the intermediate-scale demonstrator for the full IAXO concept. Its goals include technology validation (magnet design, x-ray optics, detector systems) and competitive physics reach for axion and ALP searches in certain regions of parameter space (Figure 1, ref. [16]). The calorimeter studies described in this report are part of the R&D effort to evaluate detector concepts that complement the primary X-ray detectors and broaden sensitivity to nuclear-line and supernova signals as seen in Figure 2, ref. [13].

2 Objectives

1. Quantify detector acceptance for 5.5 MeV and 100 MeV photons as a function of detector length, diameter, position (vacuum vs air), and material.
2. Implement Gaussian energy-resolution smearing to model finite detector resolution.
3. Compare shower profiles (radial/longitudinal) between gamma signals and cosmic muon backgrounds and identify possible features for background discrimination.
4. Recommend detector material and placement optimizing acceptance and cost.

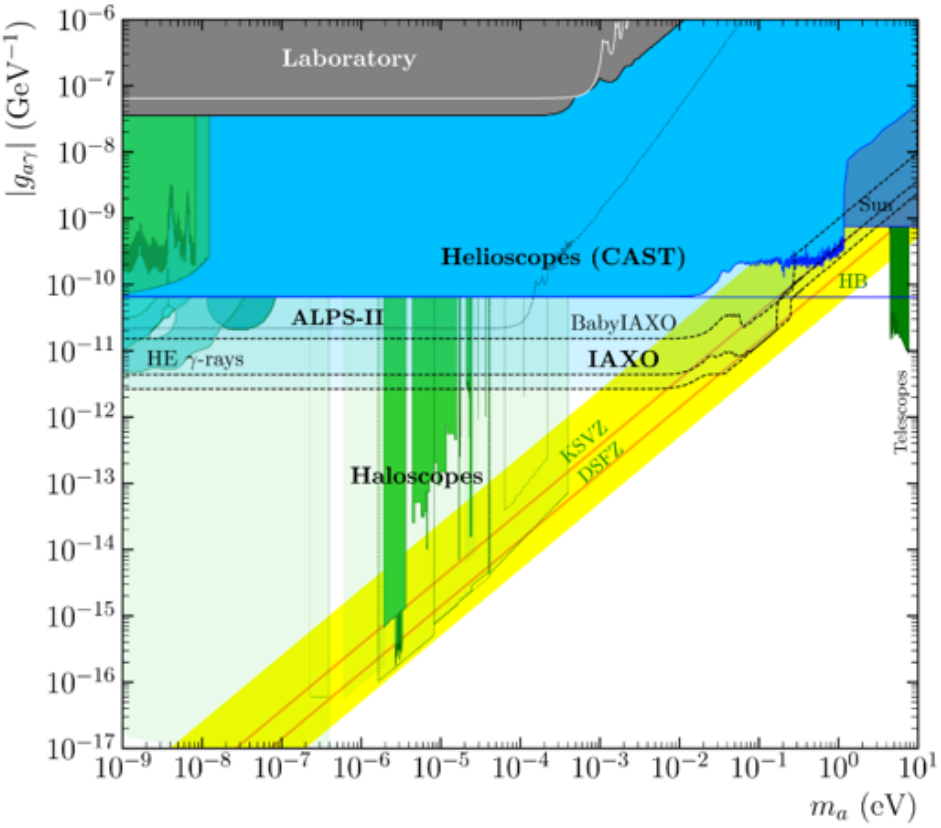


Figure 1: Axion detection sensitivity from various instruments [16]

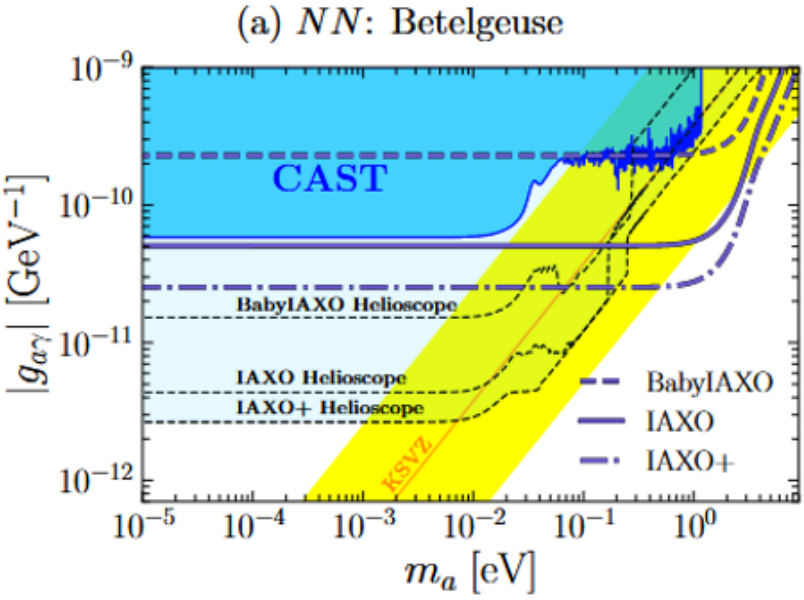


Figure 2: Axion detection sensitivity from various instruments with included supernova signal from Betelgeuse [13]

3 Acceptance Study

3.1 Methodology

While helioscope conversion is central to the overall experiment, this report treats the photon flux incident on the calorimeter as an input and focuses on calorimeter response.

Software: OpenGATE
In GATE, detectors are modeled as sensitive volumes that mimic the geometry, material, and response of real radiation detection systems, allowing one to follow the full chain from particle interaction to signal formation. When a particle enters a detector, GATE uses GEANT4 physics models to track its interactions and energy deposits, which can then be converted into optical photons in scintillators or charge carriers in semiconductors. An example of a visualization is shown in Figure 3, scattering of the rays can be seen.

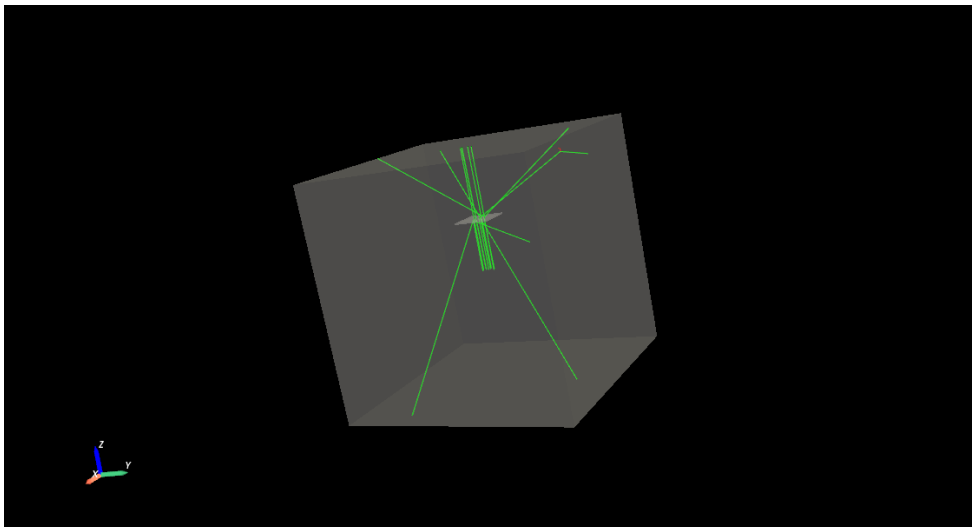


Figure 3: OpenGATE simulation example with a point source and a prism detector

- Using OpenGATE (Geant 4-based) single-photon events at target energies (5.5 MeV and 100 MeV).
- Two media configurations:
    1. **Inside cryostat (vacuum)** — no steel plate, no air.
    2. **Outside cryostat (air)** — photons must pass a steel plate and air before entering calorimeter.
- Materials tested: GAGG, NaI (Tl) (widely studied material), CsI(Tl), and Polystyrene (commercially available), in order of high to low energy resolutions; the properties and prices are listed in table 1
- Detector geometries: 70-cm diameter cylinder (diameter of the cryostat, cannot be wider than this) with varied lengths (e.g. 2–42 cm).
- Source: 70-cm diameter disk producing photon beam projecting at the detector at a specified energy.

- Event selection: energy deposition histogram from each hit events with resolution smearing (see next subsection), then apply energy cut to count accepted events.

Table 1: Detector material candidates: energy resolution and approximate price per cm^3.

Name	Density (g/cm^3)	Resolution	Price ($ / cm^3)
GAGG:Ce	6.63	$\sim$ 5–6%	\$160–200
NaI(Tl)	3.67	$\sim$ 6–7%	\$20–30
CsI (Tl)	4.51	$\sim$ 6–8%	\$10–20
PVT / PS	1.02	$\sim$ 20–25%	$<$ \$5

3.2 Energy resolution (Gaussian sampling)

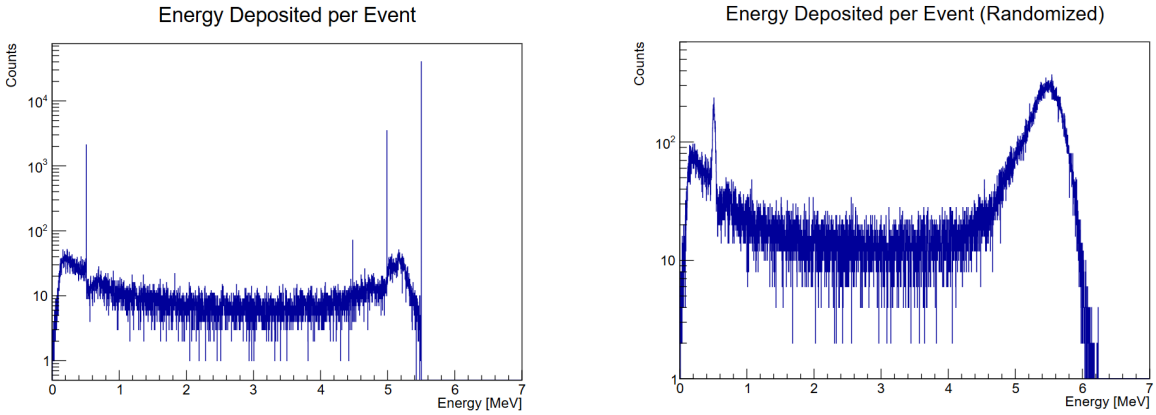
We model detector energy resolution as a Gaussian smear of the true deposited energy. Given an intrinsic resolution specified as FWHM fraction (Res, e.g. 8% for CsI(Tl) at a reference energy), we compute sigma:

$$\text{FWHM} = \text{Res} \times E, \qquad \sigma_E = \frac{\text{FWHM}}{2.355}.$$

Randomized measured energy:

$$E_{\text{meas}} = E_{\text{dep}} + \sigma_E \cdot \mathcal{N}(0, 1).$$

Implement this per-event, the results example is shown in Figure 4a and . The delta-like peaks at around 5.5 MeV from 4a are blended to one due to energy resolution of the material (CsI, 8%) as shown in Figure 4b.



(a) Before smearing

(b) After smearing (8% resolution)

Figure 4: Gamma-ray photon energy profile for CsI(Tl) at a 38 cm detector length, shown before (left) and after (right) applying an 8% energy resolution smearing.

3.3 Acceptance calculation

Acceptance A is defined at a geometry/configuration as:

$$A = \frac{N_{\text{accepted}}}{N_{\text{generated}}},$$

where an event is accepted if the measured deposited energy E_{meas} exceeds an energy cut.

For 5.5 MeV, $E_{\text{cut}} = 4.0$ MeV since natural radiativity is typically below this threshold. While for 100 MeV, E_{cut} could be set as low as 5.0 MeV since it comes from the strong signal of supernova, not expected significant background.

3.4 Results

According to Figure 5a and 5b, 5.5 MeV acceptance is greatly affected by the steel plate for the one placing outside the vacuum: the top panel shows greater acceptance in vacuum than the bottom panel (air) in which the steel plate absorbs about 40% of the incoming photons. On the other hand, the acceptance does not differ in the case of 100 MeV, as seen in Figure 6a and 6b. This is because the steel plate instead scatters the photons creating a shower, which can still be captured by the detector.

According to these results, having the detector in vacuum would be logical as it provides similar acceptance for 100 MeV but much better for 5.5 MeV ($\sim$ 40% greater).

Considering materials, GAGG provides the highest acceptance of all (green line) (as expected from the highest density and resolution), then CsI, NaI, and polystyrene (plastic) in order of acceptance. Since CsI bahaves similarly from GAGG and even has the cheaper price per volume, CsI is the most promising candidate for making a detector to detect 5.5 and 100 MeV photons.

4 Shower Profile Study

4.1 Methodology

Let coordinates be (x, y, z) with detector axis along $+z$ (5.5-MeV photon and 1-GeV muon direction is set to be $+z$ and $-y$ respectively). Variables considered are radial coordinate (r), weighted standard deviation of longitudinal energy deposition along the z-axis (σ_z), weighted standard deviation of radial energy distribution (ensemble average) (σ_r), total deposited energy per event (E_i).

Procedure:

1. For each simulated event, energy deposited is recorded in per-layer (or per-voxel) segmentation.

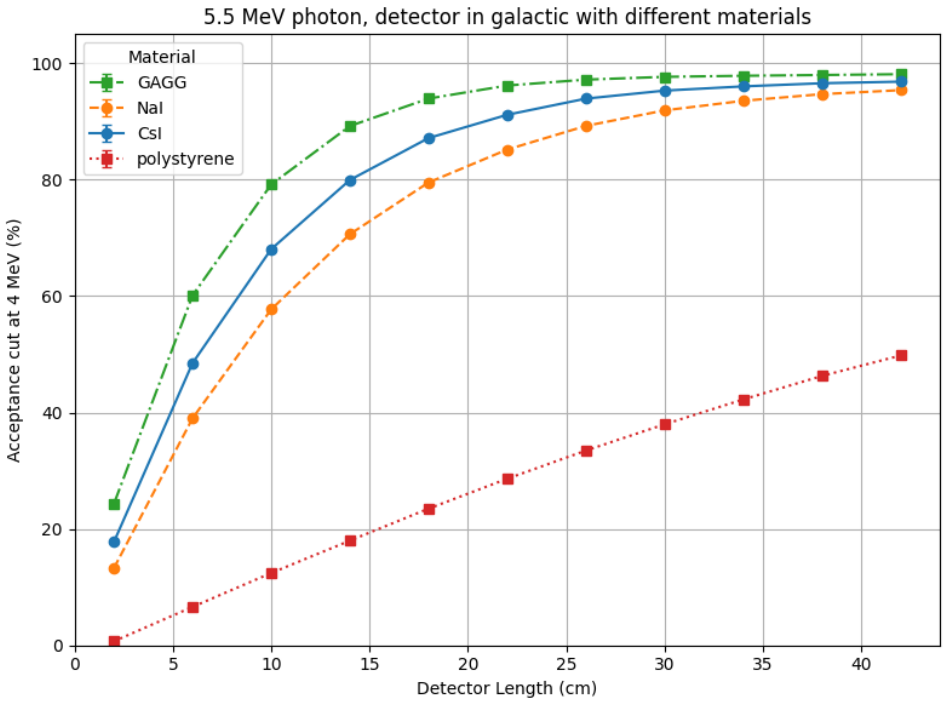
2. Each coordinate components are computed per-event, then radial moments:

$$\bar{z} = \frac{\sum_i z_i E_i}{\sum_i E_i}, \quad \sigma_z^2 = \frac{\sum_i (z_i - \bar{z})^2 E_i}{(\frac{N-1}{N}) \sum_i E_i}$$

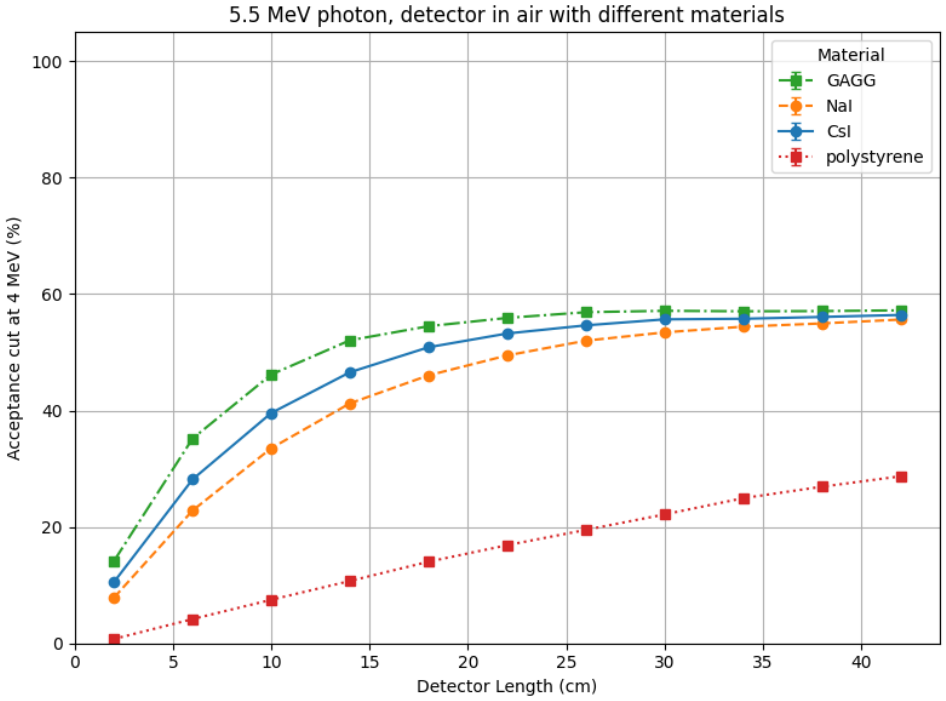
   and similarly for x, y, then

$$r = \sqrt{\bar{x}^2 + \bar{y}^2}, \quad \sigma_r^2 = \sigma_x^2 + \sigma_y^2$$

3. Profile plots are built: r vs σ_r, σ_z vs σ_r, and 5.5 MeV and cosmic muon background profiles are compared.

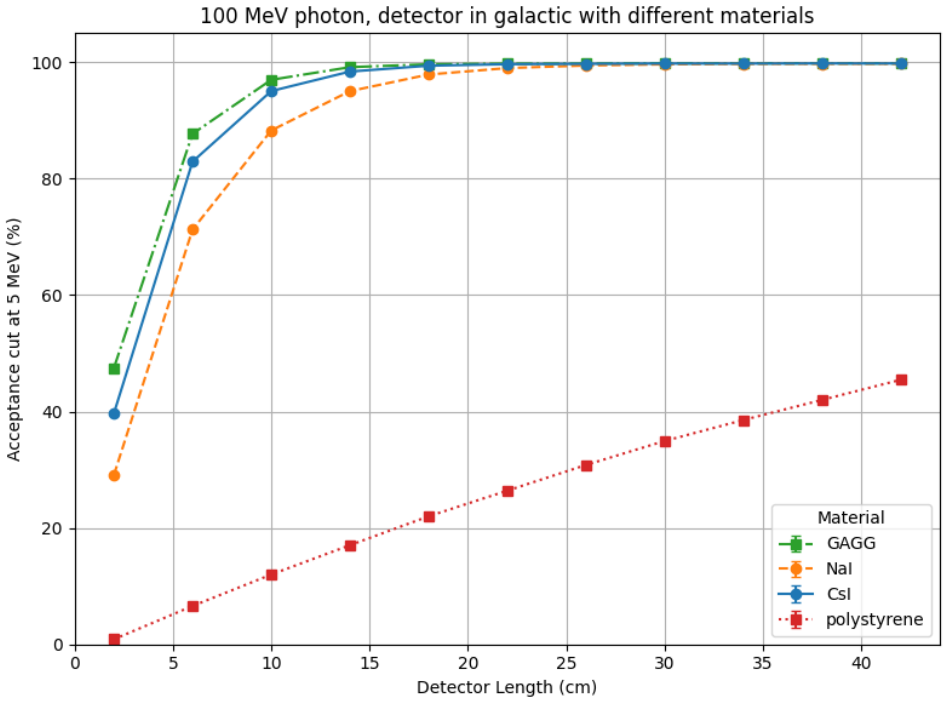


(a) Acceptance vs. Length in vacuum for 5.5 MeV photons

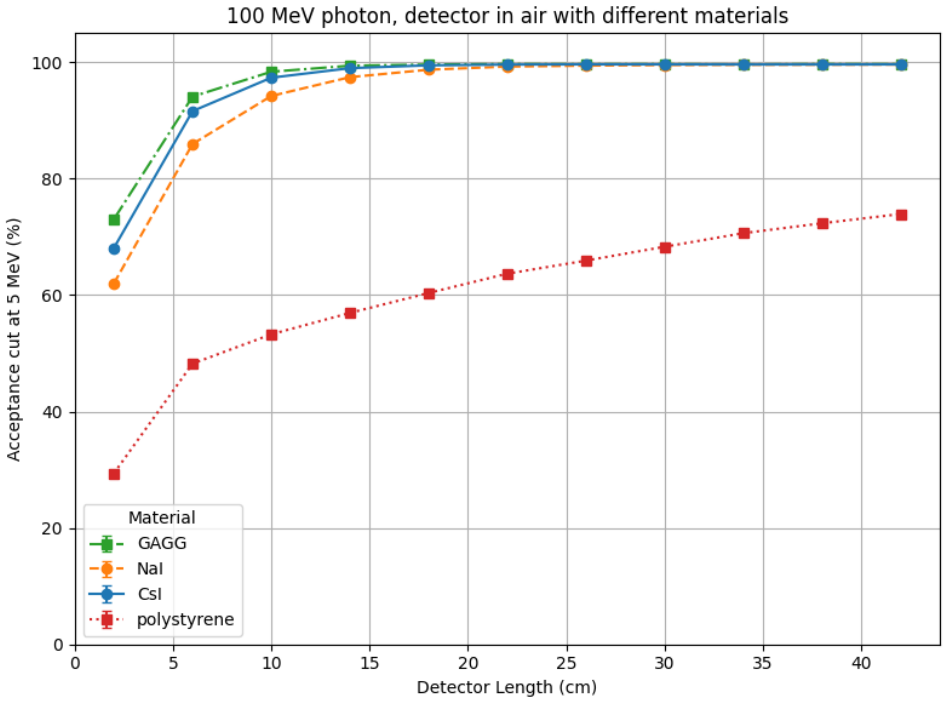


(b) Acceptance vs. Length in air for 5.5 MeV photons

Figure 5: 5.5 MeV energy response on 4 materials: GAGG, NaI, CsI, and polystyrene.



(a) Acceptance vs. Length in vacuum for 100 MeV photons



(b) Acceptance vs. Length in air for 100 MeV for 100 MeV photons

Figure 6: 100 MeV energy response on 4 materials: GAGG, NaI, CsI, and polystyrene.

4.2 Results

4.3 Key observations

According to Figure 7 and 8, it can be observed that for 5.5-MeV Photon, gammas originate from the left center and travel in $+z$, so the main spread is along the z direction (having higher values of σ_z in some region). Also, the color bar shows less energies since the maximum is only 5.5 MeV.

For cosmic muons, since they travel from the upper point toward $-y$, their displacement in the x-y plane ($r = \sqrt{x^2 + y^2}$) is dominated by the y component, causing the longitudinal spread (σ_z) approximately constant and lower than some range of gamma because of the symmetry in z-direction. The color bar is saturated at high energy.

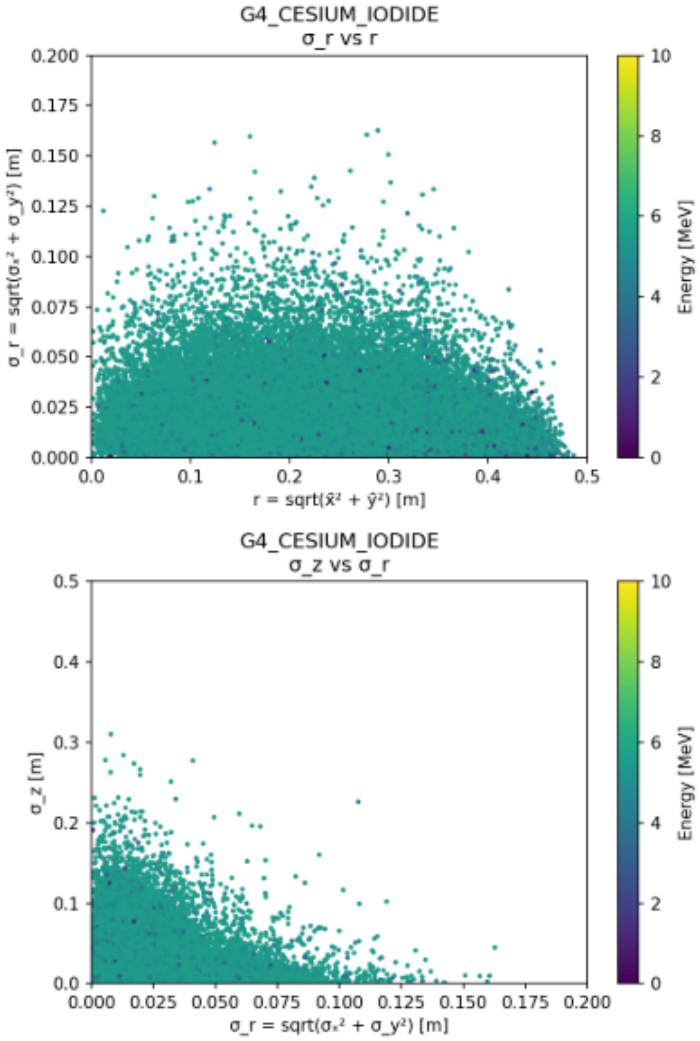


Figure 7: 5.5-MeV photon: σ_r vs. r (top), σ_z vs. σ_r (bottom)

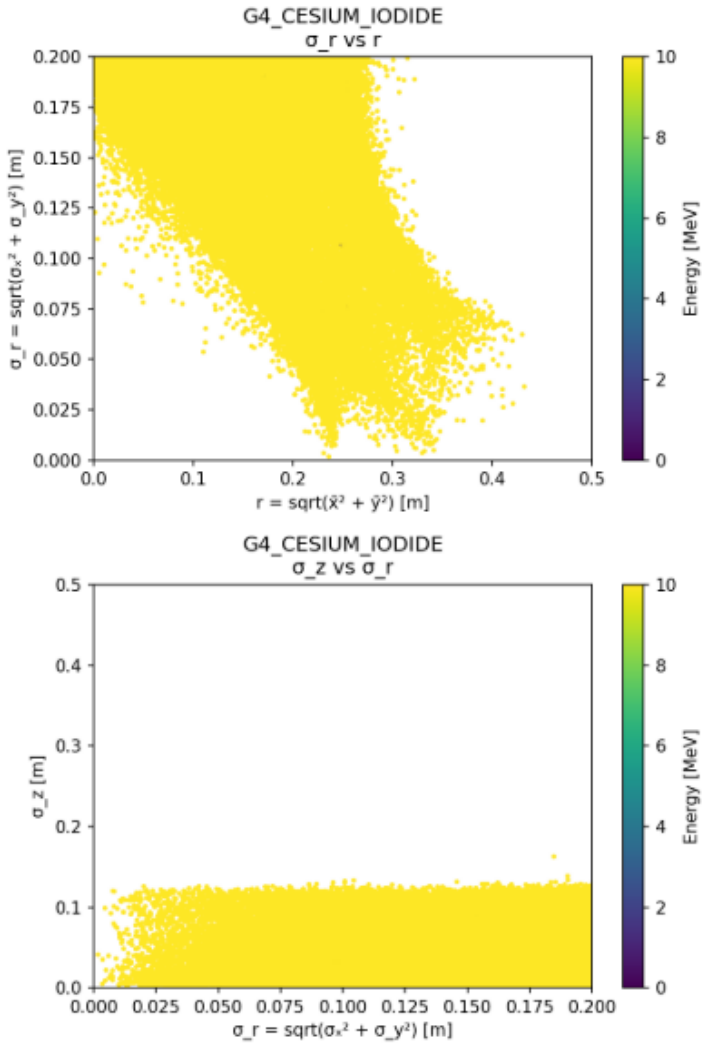


Figure 8: 1-GeV Cosmic Muon: σ_r vs. r (top), σ_z vs. σ_r (bottom)

Physical Interpretation:
Regarding cosmic muon events, the profiles are more radially dispersed in the x-y plane but have little longitudinal spread, unlike the gamma events, which appear more longitudinally dispersed (large σ_z). This reflects the difference between single-particle (muon) and shower (gamma) event topologies.

5 Conclusions

BabyIAXO has the potential to detect MeV photons with a new calorimeter, to cover a higher axion masses detection. Considering environment around the detector, The calorimeter configuration inside the vacuum (no steel plate) substantially improves acceptance than outside the vacuum for low-energy (5.5 MeV) photons — approximately 40% higher in the study. For 100 MeV photons differences between vacuum and air configurations are not significant. Regarding material, CsI(Tl) is recommended as a robust candidate (good acceptance and reasonable price) among the materials tested (CsI, GAGG, NaI, and polystyrene).

In the shower study, shower-shape and energy-scale differences between gamma signals and cosmic-muon backgrounds are significant and permit background rejection strategies. The study could be improved to the next step by considering also other possible backgrounds e.g. environmental radioactivity, rare cosmic muons and other cosmic events.

References

[1] R. D. Peccei and H. R. Quinn. Cp conservation in the presence of pseudoparticles. *Physical Review Letters*, 38:1440–1443, 1977.

[2] Steven Weinberg. A new light boson? *Physical Review Letters*, 40:223–226, 1978.

[3] Frank Wilczek. Problem of strong p and t invariance in the presence of instantons. *Physical Review Letters*, 40:279–282, 1978.

[4] Andreas Ringwald. Searching for axions and alps from string theory. *Journal of Physics: Conference Series*, 485(1):012013, 2014.

[5] K. Ehret, M. Frede, S. Ghazaryan, M. Hildebrandt, E.-A. Knabbe, D. Kracht, A. Lindner, J. List, T. Meier, N. Meyer, D. Notz, J. Redondo, A. Ringwald, G. Wiedemann, and B. Willke. New alps results on hidden-sector lightweights. *Physics Letters B*, 689(4):149–155, 2010.

[6] M. Dine, W. Fischler, and M. Srednicki. A simple solution to the strong cp problem with a harmless axion. *Physics Letters B*, 104:199–202, 1981.

[7] A. R. Zhitnitsky. On possible suppression of the axion hadron interactions. *Soviet Journal of Nuclear Physics*, 31:260–264, 1980. In Russian; English translation: Yad. Fiz. 31, 497 (1980).

[8] J. E. Kim. Weak interaction singlet and strong cp invariance. *Physical Review Letters*, 43:103–107, 1979.

[9] M. A. Shifman, A. I. Vainshtein, and V. I. Zakharov. Can confinement ensure natural cp invariance of strong interactions? *Nuclear Physics B*, 166:493–506, 1980.

[10] Georg G. Raffelt. *Stars as Laboratories for Fundamental Physics: The Astrophysics of Neutrinos, Axions, and Other Weakly Interacting Particles*. University of Chicago Press, 1996.

[11] P. W. Graham, I. G. Irastorza, S. K. Lamoreaux, A. Lindner, and K. A. van Bibber. Experimental searches for the axion and axion-like particles. *Annual Review of Nuclear and Particle Science*, 65:485–514, 2015.

[12] S. Andriamonje, S. Aune, D. Autiero, K. Barth, A. Belov, B. Beltrán, H. Bräuninger, J. M. Carmona, S. Cebrián, J. I. Collar, T. Dafni, M. Davenport, L. Di Lella, C. Eleftheriadis, J. Englhauser, G. Fanourakis, E. Ferrer-Ribas, H. Fischer, J. Franz, P. Friedrich, T. Geralis, I. Giomataris, S. Gninenko, H. Gómez, M. Hasinoff, F. H. Heinsius, D. H. H. Hoffmann, I. G. Irastorza, J. Jacoby, K. Jakovčić, D. Kang, K. Königsmann, R. Kotthaus, M. Krčmar, K. Kousouris, M. Kuster, B. Lakić, C. Lasseur, A. Liolios, A. Ljubičić, G. Lutz, G. Luzón, D. W. Miller, J. Morales, A. Ortiz, T. Papaevangelou, A. Placci, G. Raffelt, H. Riege, A. Rodríguez, J. Ruz, I. Savvidis, Y. Semertzidis, P. Serpico, L. Stewart, J. D. Vieira, J. Villar, J. Vogel, L. Walckiers, and K. Zioutas. Search for solar axion emission from ^{7}li and d(p,γ)^{3}he nuclear decays with the cast γ-ray calorimeter. *Journal of Cosmology and Astroparticle Physics*, (03):032, Mar 2010.

[13] P. Carenza, J. A. García Pascual, M. Giannotti, I. G. Irastorza, M. Kaltschmidt, A. Lella, A. Lindner, G. Lucente, A. Mirizzi, M. J. Puyuelo, and et al. Detecting supernova axions with iaxo. *Journal of Cosmology and Astroparticle Physics*, 2025(07):075, 2025.

[14] S. Andriamonje et al. An improved limit on the axion-photon coupling from the cast experiment. *Journal of Cosmology and Astroparticle Physics*, 2007(04):010, 2007.

[15] Eric Armengaud et al. Conceptual design of the international axion observatory (iaxo). *Journal of Instrumentation*, 9(05):T05002, 2014.

[16] A. Abeln et al. Conceptual design of babyiaxo, the intermediate stage towards the international axion observatory. *Journal of High Energy Physics*, 2021(5):137, 2021.